Photonics and Nanostructures – Fundamentals and Applications 29 (2018) 22–29

Contents lists available at ScienceDirect

Photonics and Nanostructures – Fundamentals and Applications

journal homepage: www.elsevier.com/locate/photonics

# Non-iridescent structural colors from uniform-sized $SiO_2$ colloids

Gökhan Topçu, Tuğrul Güner, Mustafa M. Demir*

*Department of Materials Science and Engineering, İzmir Institute of Technology, 35430, Urla, Turkey*

ARTICLE INFO

*Article history:*
Received 10 October 2017
Received in revised form 12 January 2018
Accepted 15 January 2018
Available online 4 February 2018

*Keywords:*
Aggregates
Iridescence
Non-iridescence
Orange
Photonic crystal
Photonic glass

ABSTRACT

Structural colors have recently attracted interest from diverse fields of research due to their ease of fabrication and eco-friendliness. These types of colors are, in principle, achieved by periodically arranged submicron-diameter colloidal particles. The interaction of light with a structure containing long-range ordered colloidal particles leads to coloration; this usually varies depending on the angle of observation (iridescence). However, the majority of the applications demand constant color that is independent of the viewing angle (non-iridescence). In this work, silica colloids were obtained using the Stöber method at different sizes from 150 to 300 nm in an alcoholic dispersion. The casting of the dispersion on a substrate leaves behind a photonic crystal showing a colorful iridescent film. However, centrifugation and redispersion of the $SiO_2$ particles into fresh solvent may cause the formation of small, aggregated silica domains in the new dispersion. The casting of this dispersion allows for the development of photonic glass, presumably due to the accumulation of aggregates showing stable colloidal film independent of viewing angle. Moreover, depending on the size of the silica colloids, non-iridescent photonic glasses with various colors (violet, blue, green, and *orange*) are obtained.



## 1. Introduction

Color is an important information carrier between the environment and color-sensitive living organisms. As a well-known interesting example, chameleons have the unique ability to exhibit rapid color changes when they feel danger or during social interactions such as male-dominance contests or courtship [1]. Color is, in fact, an integral part of daily life [2–9] not only for animals but also for human beings, for whom color plays an important role in art, decoration, clothing, and more. In general, three different types of mechanism are known to be responsible for color generation: 1) the absorption of a particular wavelength resulting in the reflection of others, which is responsible for the colors of flowers, paints, dyes, pigments, etc. [10]; 2) emission at specific wavelengths such as LEDs [11,12]; and 3) structural colors [13] based on the diffraction, scattering, and dispersion of light as a result of its interaction with the structured materials. The first method suffers from photobleaching [14,15], toxicity [16], and poor color quality due to absorption and reflection. Coloration as a result of the second method can provide bright and pure colors but requires external power supplies. The third mechanism, by contrast, shows no photobleaching [17] and can generate a wide range of colors [18,19] in non-toxic and environmentally friendly ways.

Structural color is a well-known phenomenon that is commonly observed in nature, e.g., *Morpho* butterflies [20], beetles, etc. [21,22], and attracts great attention [13,23–27]. These types of colors can be divided into two groups depending on their behavior with respect to the angle of observation: iridescent [23,25,28,29] and non-iridescent [30,31]. The former offers colors that are generated from structures that contain periodically arranged nano- or microparticles, depending on the observation angle (iridescence). These periodically arranged and colored structures are called *photonic crystals*. By contrast, the latter possesses a quasi-ordered arrangement of colloids called *photonic glass* and offers the opposite: angle-independent color generation (non-iridescence). In this case, unlike the photonic crystal, the arrangement of the colloidal particles shows a glassy structure with a short-range order. This type of color finds a wide range of potential applications including reflective displays, colorimetric sensors, textiles, etc. [17,30,32–37]. In general, various methods have been developed for the generation of non-iridescent structural color using polymeric or inorganic colloidal systems [17,30,31,38–44]. For instance, Takeoka et al. reported [17] the formation of non-iridescent film using uniform $SiO_2$ colloidal particles of 280–360 nm diameter by spraying. It was argued that fast solvent evaporation in the course of the spraying process allows the formation of a colloidal amorphous array, which is, in fact, the main requirement for non-iridescence. The

* Corresponding author.
*E-mail address:* mdemir@iyte.edu.tr (M.M. Demir).

https://doi.org/10.1016/j.photonics.2018.01.002
1569-4410/

clogging of the spraying nozzle appears to be a common problem in the processing of colloidal dispersions. Harun-Ur-Rashid et al. [45] achieved the amorphous array by mixing two monodispersed $SiO_2$ colloids with two populations of different sizes, 220 and 310 nm. While the large colloidal particles formed the periodic structure, the small ones were employed to deteriorate the regularity of the colloidal crystal arrangement. Silica is an inexpensive, abundant, and easily prepared material [46], and it is also capable of being frequently associated with functional counterparts. As an example, Wang et al. [47] employed ZnS as a core encapsulated by $SiO_2$ to achieve saturated emission. ZnS is a typical II–VI type of semiconductor that produces bright and intense emissions in visible regions. Another metal oxide core, the $SiO_2$ shell system, has been reported by Lee et al. [48]. The authors employed an $Fe_3O_4$ core to obtain both structural color and magnetic response from the resulting colloidal film. Apart from binary material components, using a unary system, for instance merely uniform-sized $SiO_2$ colloidal particles without involving a secondary material may simplify the formation of photonic glass with non-iridescent color. In this study, non-iridescent color was achieved using just $SiO_2$ colloids. The preparation of $SiO_2$ colloidal films includes the isolation of monodispersed colloids and their redispersion into fresh solvent as aggregated-colloidal particle domains. Then, the photonic glass is obtained by evaporating the redispersed colloids over a substrate. Moreover, the colloidal particles with a diameter of 150–300 nm generate various angle-independent colors such as violet, blue, green, or orange depending on the particle size. This approach offers a facile way of generating non-iridescent colors that can readily be applied to other fields of application.

## 2. Experiment

### 2.1. Materials

Tetraethyl orthosilicate (TEOS, >99.9%, Sigma-Aldrich) and ammonia solution (25%, Sigma-Aldrich) were purchased and used with no further purification. Ethanol (EtOH, >96%, Tekkim) was employed as a solvent. The residual moisture in the reactants and solvent was removed using a molecular sieve (4 Å pore size).

### 2.2. Synthesis of $SiO_2$ colloids

Monodispersed $SiO_2$ colloids were synthesized using a modified Stöber method [49]. Initially, the mother solution containing ammonia (in a range between 2–1 mL) and EtOH (in a range between 40–15 mL) was prepared in an Erlenmeyer flask and homogenized for 5 min. Subsequently, TEOS (1 mL) was added to the mixture, and the reaction was maintained at room temperature for 1 h. The $SiO_2$ particles were collected by centrifugation (6000 rpm for 5 min) and washed with EtOH three times to eliminate unreacted TEOS and ammonia. The isolated $SiO_2$ particles were then redispersed into EtOH while fixing the concentration of redispersed particles as 5 mg/mL.

### 2.3. Preparation of photonic films

Photonic crystals were obtained through the sedimentation of the as-synthesized colloidal particles on a substrate upon solvent evaporation. An aliquot of the (4 mL) $SiO_2$ colloids mentioned above was cast onto a Petri dish (diameter: 5 cm). Drying of colloids was carried out at room temperature under 200 mbar for 24 h. In contrast, photonic glasses were prepared in two steps: i) isolation of the colloids by centrifugation (6000 rpm for 5 min) and ii) redispersion of the colloids into fresh EtOH. The resulting dispersion was cast on a substrate; an assembly of the silica colloids was obtained after solvent evaporation.

### 2.4. Characterization

The pH was measured during colloid synthesis using a multimeter (pHenomenal® MU 6100 L, VWR International, Vienna, Austria). Particle size was determined using Dynamic Light Scattering (DLS; Zetasizer Nano ZS, Malvern Instruments, Worcestershire, UK). The $SiO_2$ colloidal particles were observed by Scanning Electron Microscopy (SEM; Quanta 250, FEI, Hillsboro, OR, USA). Images of the photonic films were captured by camera (Canon EOS 5D, Tokyo, Japan). The reflection spectra of the photonic films were recorded by spectrometer (USB2000+, Ocean Optics Inc., Dunedin, FL, USA) via premium fiber cable.

## 3. Results & discussion

### 3.1. Synthesis of $SiO_2$ colloids

TEOS is the source of silica. It is hydrolyzed in a alkali reaction medium such that $-OC_2H_5$ groups are readily substituted with $-OH$ that leads to the formation of silicic acid, $Si(OH)_4$. The pH of the medium accordingly decreases from 11.3 to 10.7 (Fig. 1**a**). The condensation of $Si(OH)_4$ develops upon the formation of silica clouds. When the $SiO_2$ clouds reach a critical mass, which is considered to be 2–3 nm diameter, nuclei are born [50]. The consumption of the $-OH$ group causes a slight increase of pH to 11.0. The nuclei are insoluble primary particles and tend to aggregate in an alkali medium to reduce their surface area. Hence, larger colloidal particles begin to form as a result of their association. Fig. 1**(b–e)** shows SEM images of the colloidal particles prepared at various TEOS:EtOH compositions. The size of the colloids gets larger as the concentration of TEOS increases. Table 1 presents the synthesis conditions and the feature of the resulting colloids. A direct correlation was found between the amount of EtOH and the diameter of the $SiO_2$ colloidal particles. As the amount of EtOH increases, the mean diameter of the colloidal particles is reduced from 301 to 157 nm, most probably due to the dilution of the reactants. The fifth column of Table 1 shows the results of the same colloidal dispersion obtained by DLS. The number average size distributions are given in Fig. 1**f**. Consistent with the results obtained by microscopy, there is a systematic decrease of the mean diameter of the colloids by increasing the amount of solvent (EtOH). The distributions are uniform and Gaussian type. Note that the size obtained by DLS is nearly 20% larger than that obtained by microscopy. The difference may be based on the fact that the diameter in SEM is measured in a vacuum while DLS measures the hydrodynamic diameter (*Rh*) of the colloidal particles in solvent. Since the silanol groups on the surface of the colloidal particles form hydrogen bonds with surrounding water molecules, they appear larger in DLS than the corresponding particles in a dry state (SEM). The inset of Fig. 1**a** shows a representative $SiO_2$ dispersion. Independent of the size, the dispersions are milky due to optical scattering of the colloidal particles. Pseudo-aggregates of colloidal particles were obtained after centrifugation and redispersion steps. To verify the existence

**Table 1**
The features of the silica colloids at various conditions.

| | ratio (v:v) | | | | | |
|---|---|---|---|---|---|---|
| | EtOH | TEOS | $d_{SEM}$ (nm) | $d_{DLS}$ (nm) | PDI | $\lambda_{refl.}$ (nm) |
| $SiO_2$-*violet* | 40 | 1 | 157 | 181 | 0.021 | 380 |
| $SiO_2$-*blue* | 30 | 1 | 204 | 236 | 0.011 | 435 |
| $SiO_2$-*green* | 20 | 1 | 233 | 279 | 0.019 | 498 |
| $SiO_2$-*orange* | 10 | 1 | 301 | 347 | 0.029 | 578 |

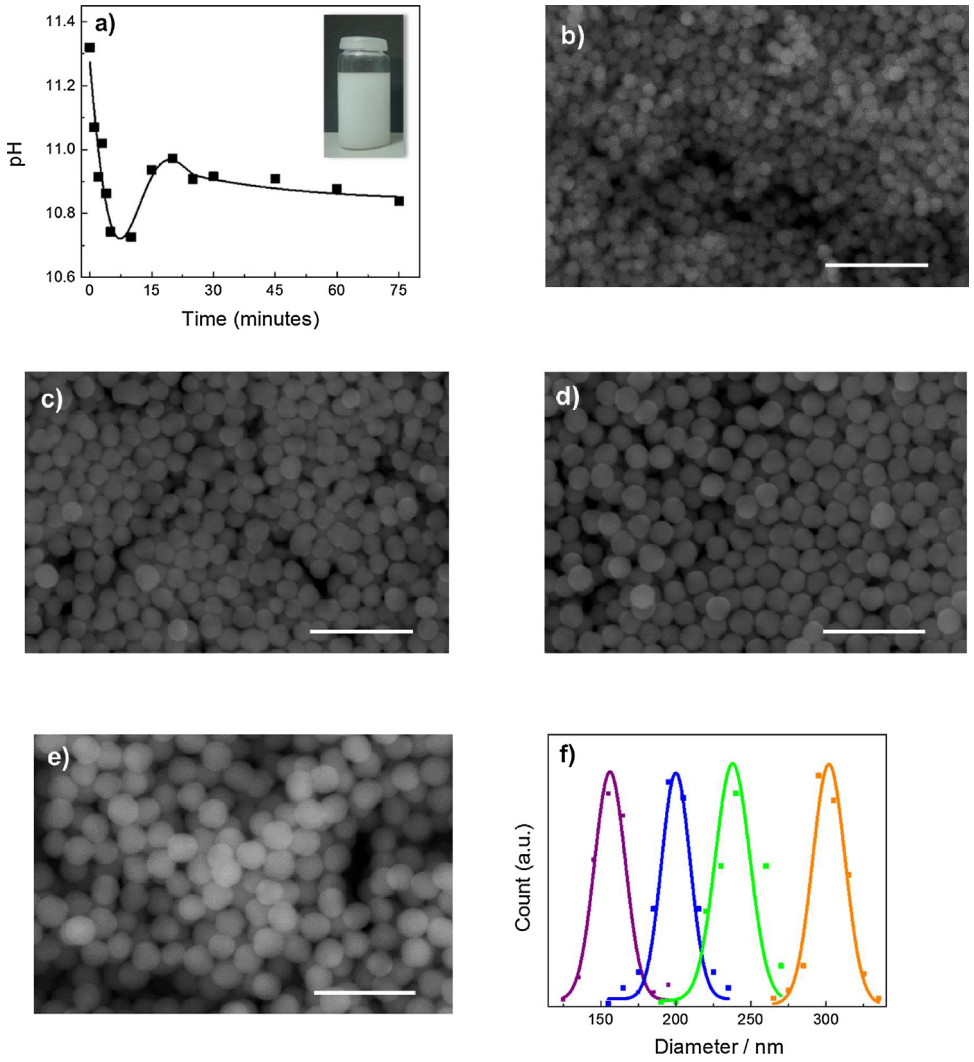


**Fig. 1.** a) pH of the reaction medium in the course of $SiO_2$ synthesis. The inset shows photographic image of representative colloidal silica dispersion. SEM images of various size $SiO_2$ colloids. Scale bar indicates 1 μm. [b) $SiO_2$-*violet*, c) $SiO_2$-*blue*, d) $SiO_2$-*green* and e) $SiO_2$-*orange*]; (f) particle size distributions ($d_{SEM}$) of the $SiO_2$ colloidal particles in various ratio of EtOH:TEOS. (For interpretation of the references to color in this figure legend, the reader is referred to the web version of this article.)

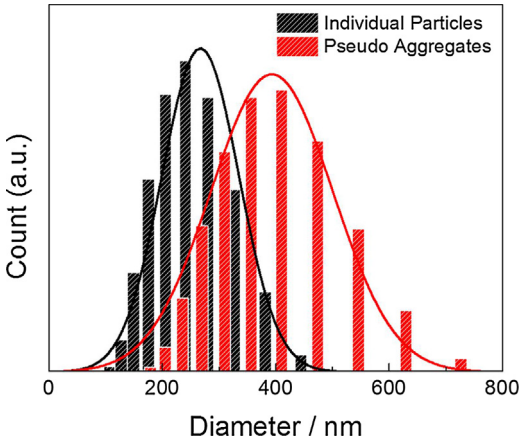


**Fig. 2.** Size distribution of individual colloidal particles and pseudo aggregates of $SiO_2$-*blue* in EtOH dispersion.

of the aggregates, the DLS method was used since it provides information over the entire population in dispersion. Fig. 2 shows the size distribution of both $SiO_2$-blue individual colloidal particles and their pseudo-aggregates. The average hydrodynamic diameter (*Rh*) of as-synthesized particles was found to be 236 nm, while the aggregated ones were measured to be almost 400 nm. Furthermore, the polydispersity index (PDI) increased from 1.1% to 10%. These results indicate that aggregated-colloidal domains were formed as a result of centrifugation and maintained their aggregated-colloidal domains even after redispersion.

### 3.2. Iridescent color of photonic crystals

The as-synthesized colloidal dispersion is cast on a glass substrate. Solvent evaporation at room temperature leaves behind a photonic crystal film composed of $SiO_2$ colloidal particles. Fig. 3 shows photos and spectra of the resulting representative photonic crystal at various angles. The upper frame (Fig. 3**a**) shows that the same film changes color from yellow to blue depending on the angle of observation. Fig. 3**b** shows the reflection spectra of the photonic crystal at various angles. The shape of the spectrum and the wavelength corresponding to maximum intensity were found to vary. The wavelengths at maximum intensity change from 570 nm to 425 nm (blue shifting) as the angle increases. Iridescent color satisfies the following Bragg-Snell equation:

$$\lambda_{max} = 2d_{(111)}\sqrt{\left(n_{eff}{}^2 - sin^2\theta\right)} \quad (1)$$

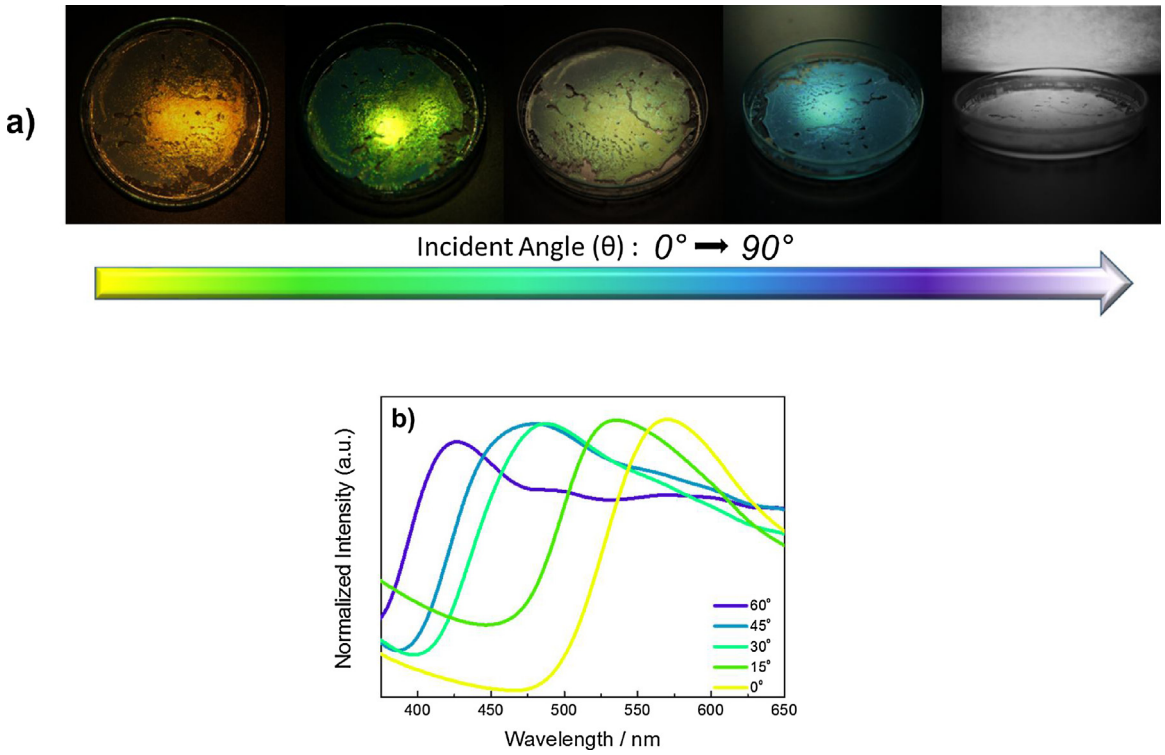


**Fig. 3.** (a) Photographs and (b) reflection spectra of the **iridescent** photonic crystal film at various angles. (For interpretation of the references to color in this figure legend, the reader is referred to the web version of this article.)

Obviously, the wavelength of the reflected light depends on the incident angle $\theta$, the lattice spacing of the fcc structure $d_{(111)}$ (corresponding to the close-packed structure), $n_{eff}$ and the effective refractive index.

The index is considered to be additive on the basis of the volume fraction of silica and air. The parameters ($d_{(111)}$ and $n_{\text{eff}}$) can be calculated as follows:

$$d_{(111)} = \left(\sqrt{3}/2\right) D \tag{2}$$

$$n_{eff} = \left(n_s{}^2 f_s + n_{air}{}^2 (1 - f_s)\right)^{1/2} \tag{3}$$

where the diameter of the silica sphere $D$ is 262 nm, and the refractive index of silica ($n_s$) and air ($n_{air}$) are 1.45 and 1.00, respectively; $f_s$ refers to the filling ratio of colloidal silica particles in crystal that is 0.74 for the close-packed fcc structure. Theoretically, calculated $\lambda_{\max}$ are found as changing from 566 to 430 nm in the case of using the same observation angles above, which are compatible with the obtained wavelengths from the observation.

An overview SEM image of the photonic crystal film is provided in Fig. 4**a**. Colloidal particles are arranged periodically that lead to a long-range structural order. A *Fast Fourier Transform (FFT)* was run through this electron micrograph using ImageJ. Sharp spots were observed in the resulting frequency distribution (Fig. 4**b**). This method transforms the geometric structure of a given image from a spatial into a frequency domain, thereby obtaining sharp spots at certain frequencies indicating the existence of structural periodicity. In this case, sharp spots verified the close-pack ordered formation of the colloidal particles in the crystal. Monodispersed colloidal $SiO_2$ particles allow the formation of ordered structure at a long-range since they are able to fill the gaps due to their matching size [9,25,26,28].

### 3.4. Non-iridescent color of photonic glasses

In order to obtain photonic glass, the as-synthesized $SiO_2$ colloids initially were subjected to centrifugation. Fresh solvent (EtOH) was added onto the resulting colloidal precipitate such that the colloids were redispersed into the solvent volume. It is known that once the colloidal particles are isolated and packed, it is difficult to redisperse them as individual particles because they have already reduced their surface energy by aggregation. Thus, the aggregates of individual particles inevitably appear in the dispersion along with individual particles [51]. The casting of this dispersion over a substrate provides a colloidal film where the arrangement of the particles is not well ordered, contrasting to the structure of the photonic crystal; rather, a quasi-ordered structure is developed. Fig. 4**c** shows the SEM image of the film prepared by the redispersed $SiO_2$ colloidal particles. The frequency domain obtained after running FFT over this electron micrograph demonstrates that there are no sharp spots (Fig. 4**d**). This means that the geometric structure of the given image contains no structural periodicity to transform it into certain frequencies. Therefore, this result suggests the absence of a periodic arrangement of the colloidal particles, i.e., there is no long-range structural order in the photonic film. Unlike the individual particles in Fig. 4**a**, aggregated-colloidal particle domains (Fig. 4**c**) cannot be accumulated in compact packing due to the mismatch of the size of the colloidal domains. In other words, centrifugation and redispersion cause the formation of silica colloidal aggregates and allow them to accumulate randomly.

Although the colloidal particles forming the representative photonic films (crystal and glass) were synthesized in one pot, the average size of these colloidal particles in the film was found to differ; it is larger ($d$ = 262 nm) in the case of photonic crystal than in the photonic glass ($d$ = 204 nm). This difference can be attributed to the presence of residual $NH_3$ and TEOS in the colloid that was used as-synthesized. These raw materials cause the growth of col-

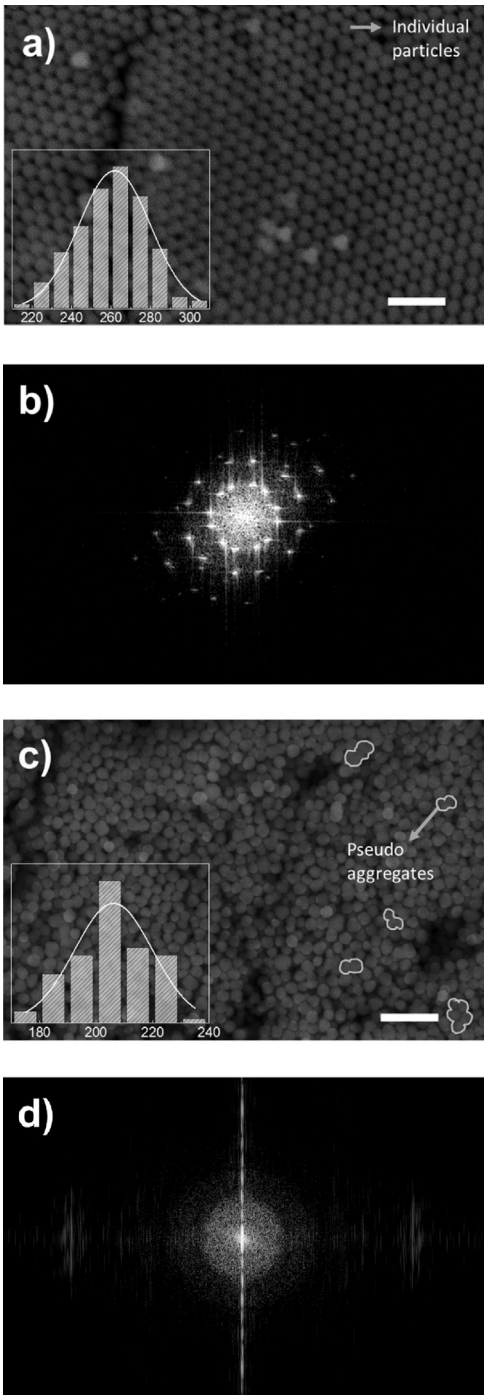


**Fig. 4.** SEM image and corresponding FFT pattern of photonic crystal (**a** and **b**) and blue photonic glass films (**c** and **d**) (Size distributions of particles are represented as inset. Scale bars indicate 1 μm).

loidal particles even during the photonic crystal formation. Since the product was washed out during centrifugation, $NH_3$ and TEOS are diminished so that the growth retards during the preparation of photonic glass.

Fig. 5**a** shows the photographic image of photonic glasses prepared by this approach (centrifugation and re-dispersion of the colloidal dispersion) at various angles of observation. The resulting films have violet, blue, green and orange colors and do not vary depending on the angle of viewing. Unlike the spectral feature of the photonic crystal film shown in Fig. 3**b**, both the shape and $\lambda_{max}$ of the reflection spectra (signals assigned with *) of the films in Fig. 5**b**–**e** remained almost unchanged with respect to observation angle, suggesting the generation of the non-iridescent color. This approach was successfully applied to the fabrication of other visible colors by simply controlling the size of the colloidal particles. For instance, Fig. 5**d** and **e** present the reflection spectra (normalized with respect to the maxima of the long wavelength signal) of the photonic glass prepared by $SiO_2$ colloids 233 and 301 nm in diameter. These films have green and orange colors, respectively. The spectra of both samples have two reflection signals; as an example, orange film show signals at 400 and 575 nm. The placement of the signals remains almost unchanged for all angles of observation employed. Fig. 6**a** shows the photographic images of the photonic glasses prepared by silica colloids of various sizes from 157 to 301 nm. As the diameter increases, non-iridescent colors are shifted from violet to orange. Fig. 6**b** presents the reflection spectra of these photonic films. It can be seen that violet and blue colors show a single signal inside the visible range. However, for green and orange colors, two signals appear. As in the case of orange, a similar set of signals at 385 and 500 nm is observed in green. The reflection signal at long wavelengths is primarily due to coherent scattering from the particle assembly. By contrast, the origin of reflectivity at short wavelengths is a topic of debate in the literature. Attempts have been made to understand the occurrence of this signal because the structural color in photonic glasses arises from the combination of both signals [45,52–54] and plays a significant role in the fabrication of non-iridescent structural colors. Noh et al. [55,56] reported the effect of multiple (single and double) scattering. The authors claimed that the appearance at short wavelengths results from the double scattering of light by the correlated structures in the short range. This scattering could be one possible reason for this poor color saturation observed at longer wavelengths, particularly in red. Another possible reason could be the single particle resonance that may develop multiple scattering in such colloidal materials. Manoharan's group pointed out that the scattering behavior of the constituent individual particles plays a key role. The interference of light inside the particles leads to enhanced scattering at wavelengths other than those related to the interparticle correlations. Individual particles backscatter light arising from cavity modes more strongly in blue; thus, it is difficult to achieve angle-independent red in structural color. For violet and blue non-iridescent colors, the scattered light from the particles falls into the UV region that does not affect the resulting color, at least taking into account the perception of the human eye. However, in the case of longer wavelengths, scattered light from individual particles starts to fall into the visible range, particularly around the blue region. This scattering may reduce the color saturation and can even shift the perceived color toward blue [57]. In this sense, the fabrication of violet, blue, or green non-iridescent colors is easier and more common compared to red color generation in nature.

The wavelengths showing maximum intensity ($\lambda_{max}$) as a function of incident angle $\theta$ are presented in Fig. 7**a.** Filled black circles represent the colloidal film prepared by individually dispersed $SiO_2$ colloidal particles, while squares refer to the one obtained by redispersed silica colloids. In the former case, wavelengths are found to decrease with the increasing observation angle (iridescence). More than a 100 nm shift is evident in $\lambda_{max}$ depending on the angle of observation from $0^0$ to $60^\circ$. However, in the latter one, the wavelength remains unchanged with respect to the incident angle $\theta$ (non-iridescence). The *International Commission on Illumination* (CIE) 1931 chromaticity diagram is shown in Fig. 7**b.** As the incident angle $\theta$ increases, the generated color shifts from red to blue for iridescent film; however, it remains almost unchanged at the blue region at every angle for the non-iridescent one.

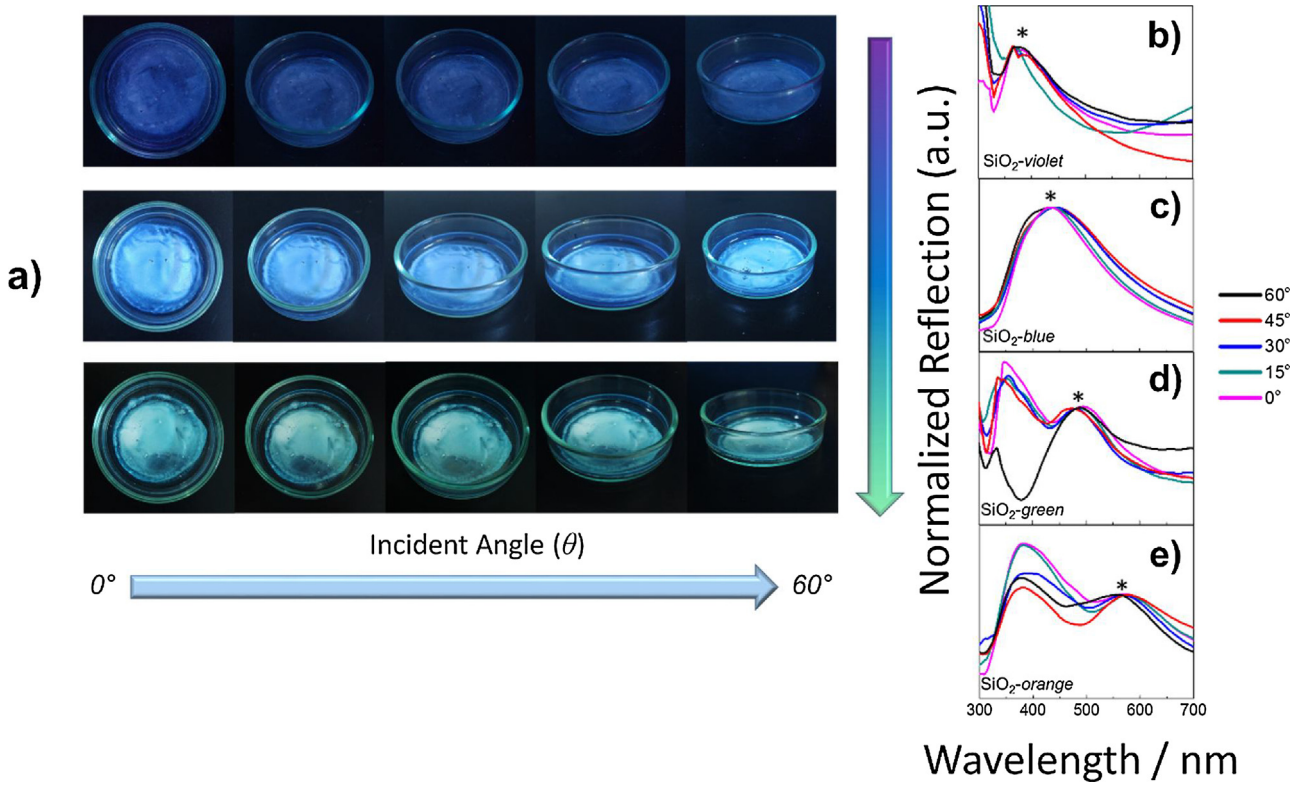


**Fig. 5.** (a) Photographs of the **non-iridescent** violet, blue, and green photonic glasses. The reflection spectra of quasi-ordered photonic glass films at various angles, (b) violet, (c) blue, (d) green, and (e) orange. (* symbols refer to signals of main color originated from coherent reflection). (For interpretation of the references to colour in this figure legend, the reader is referred to the web version of this article.)

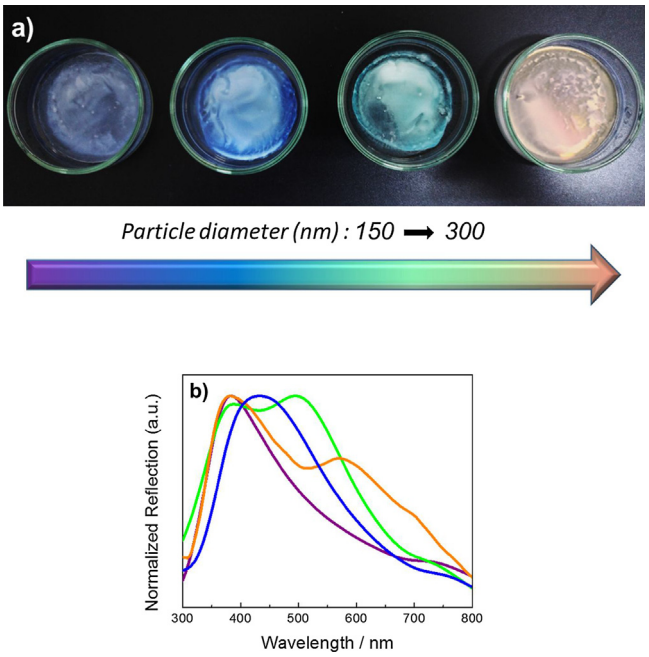


**Fig. 6.** (a) Photographs of the **non-iridescent** photonic glass films that are formed by $SiO_2$-violet, $SiO_2$-blue, $SiO_2$-green, and $SiO_2$-orange. (b) Reflection spectra of the resulting films. (For interpretation of the references to colour in this figure legend, the reader is referred to the web version of this article.)

## 4. Conclusion

In this study, non-iridescent photonic glass of various colors, i.e., violet, blue, green, and *orange* were prepared from silica colloids. Colloids of submicrometer size (150–300 nm) were obtained by the traditional Stöber method. The casting of the as-synthesized silica colloids on a solid substrate allows the production of photonic crystal. The crystal exhibits an iridescent color. The redispersion of the isolated particles into fresh solvent develops aggregated-colloidal particle domains. Therefore, casting of the redispersion does not allow the formation of long-range order; rather, it leads to a quasi-ordered photonic glass. The color of the resulting films is independent of the angle of observation (non-iridescent). In other words, a single centrifugation step in the procedure makes a clear

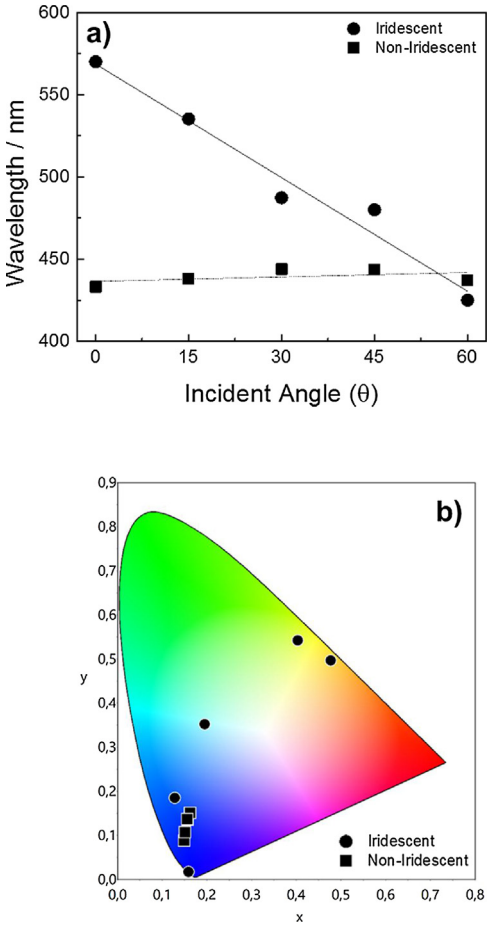


**Fig. 7.** (a) $\lambda_{max}$ of both photonic glass (non-iridescent blue) and photonic crystal (iridescent) film as a function of incident angle. (b) CIE coordinates of the both photonic films. (For interpretation of the references to colour in this figure legend, the reader is referred to the web version of this article.)

difference in the arrangement of the colloidal particles. The size of the individual colloidal particles is still the dominant parameter in the determination of the non-iridescent structural color. As the particle size increases, the obtained non-iridescent color shifts toward orange. Considering the absence of long-wavelength non-iridescent structural colors in nature, this method can be a reliable approach (centrifugation and redispersion) for obtaining an angle-independent orange color at 575 nm. This approach may have potential applications in paints, cosmetics, textiles, and displays.

## Acknowledgements

MMD acknowledges *Outstanding Young Investigator* grant of Turkish Academy of Sciences (Gebip 2013). The authors thank Ö. Şener for high quality imaging of the colloidal films.

## References

[1] J. Teyssier, S.V. Saenko, D. Van Der Marel, M.C. Milinkovitch, Photonic crystals cause active colour change in chameleons, Nat. Commun. 6 (2015) 6368.
[2] A. Kristensen, J.K. Yang, S.I. Bozhevolnyi, S. Link, P. Nordlander, N.J. Halas, N.A. Mortensen, Plasmonic colour generation, Nat. Rev. Mater. 2 (2016) 16088.
[3] Y. Fu, C.A. Tippets, E.U. Donev, R. Lopez, Structural colors: from natural to artificial systems, Wires Nanomed. Nanobiotechnol. 8 (2016) 758–775.
[4] P.V. Braun, Materials science: colour without colourants, Nature 472 (2011) 423–424.
[5] P. Ball, Bright Earth: Art and the Invention of Color, University of Chicago Press, 2003.
[6] H. Zollinger, Color Chemistry: Syntheses, Properties, and Applications of Organic Dyes and Pigments, John Wiley & Sons, 2003.
[7] R.C. Schroden, M. Al-Daous, C.F. Blanford, A. Stein, Optical properties of inverse opal photonic crystals, Chem. Mater. 14 (2002) 3305–3315.
[8] F. Marlow, P. Sharifi, R. Brinkmann, C. Mendive, Opals: status and prospects, Angew. Chem. Int. Ed. 48 (2009) 6212–6233.
[9] J.D. Joannopoulos, S.G. Johnson, J.N. Winn, R.D. Meade, Photonic Crystals: Molding the Flow of Light, Princeton University press, 2011.
[10] S. Özçelik, M.M. Demir, B. Birkan, Probing nanoscale domains of J-aggregates deposited on a mica surface, J. Phys. Chem. B 108 (2004) 4679–4683.
[11] T. Güner, D. Köseoğlu, M.M. Demir, Multilayer design of hybrid phosphor film for application in LEDs, Opt. Mater. 60 (2016) 422–430.
[12] T. Güner, U. Sentürk, M.M. Demir, Optical enhancement of phosphor-converted wLEDs using glass beads, Opt. Mater. 72 (2017) 769–774.
[13] S. Kinoshita, S. Yoshioka, J. Miyazaki, Physics of structural colors, Rep. Prog. Phys. 71 (2008) 076401.
[14] M.P. Colombini, A. Andreotti, C. Baraldi, I. Degano, J.J. Łucejko, Colour fading in textiles: a model study on the decomposition of natural dyes, Microchem. J. 85 (2007) 174–182.
[15] E. Ghelardi, I. Degano, M.P. Colombini, J. Mazurek, M. Schilling, H. Khanjian, T. Learner, A multi-analytical study on the photochemical degradation of synthetic organic pigments, Dyes Pigm. 123 (2015) 396–403.
[16] I. Lundberg, R. Milatou-Smith, Mortality and cancer incidence among Swedish paint industry workers with long-term exposure to organic solvents, Scand. Work Environ. Health (1998) 270–275.
[17] Y. Takeoka, S. Yoshioka, A. Takano, S. Arai, K. Nueangnoraj, H. Nishihara, M. Teshima, Y. Ohtsuka, T. Seki, Production of colored pigments with amorphous arrays of black and white colloidal particles, Angew. Chem. Int. Ed. 52 (2013) 7261–7265.
[18] D. Graham-Rowe, Tunable structural colour, Nat. Photonics 3 (2009) 551.
[19] M.G. Han, C.G. Shin, S.J. Jeon, H. Shim, C.J. Heo, H. Jin, J.W. Kim, S. Lee, Full color tunable photonic crystal from crystalline colloidal arrays with an engineered photonic stop-band, Adv. Mater. 24 (2012) 6438–6444.
[20] A. Ingram, A. Parker, A review of the diversity and evolution of photonic structures in butterflies, incorporating the work of John Huxley (The Natural History Museum, Londonfrom 1961–1990), Philos. Trans. R. Soc. B 363 (2008) 2465–2480.
[21] M. Srinivasarao, Nano-optics in the biological world: beetles, butterflies, birds, and moths, Chem. Rev. 99 (1999) 1935–1962.
[22] R.A. Potyrailo, H. Ghiradella, A. Vertiatchikh, K. Dovidenko, J.R. Cournoyer, E. Olson, Morpho butterfly wing scales demonstrate highly selective vapour response, Nat. Photonics 1 (2007) 123–128.
[23] S. Kinoshita, S. Yoshioka, Structural colors in nature: the role of regularity and irregularity in the structure, ChemPhysChem 6 (2005) 1442–1459.
[24] Y. Zhao, Z. Xie, H. Gu, C. Zhu, Z. Gu, Bio-inspired variable structural color materials, Chem. Soc. Rev. 41 (2012) 3297–3317.
[25] P. Vukusic, J.R. Sambles, Photonic structures in biology, Nature 424 (2003) 852–855.
[26] J.P. Vigneron, P. Simonis, Natural photonic crystals, Phys. B 407 (2012) 4032–4036.
[27] A.G. Dumanli, T. Savin, Recent advances in the biomimicry of structural colours, Chem. Soc. Rev. 45 (2016) 6698–6724.
[28] H. Cong, B. Yu, S. Wang, L. Qi, J. Wang, Y. Ma, Preparation of iridescent colloidal crystal coatings with variable structural colors, Opt. Express 21 (2013) 17831–17838.
[29] S. Yoshioka, E. Nakamura, S. Kinoshita, Origin of two-color iridescence in rock dove's feather, J. Phys. Soc. Jpn. 76 (2007) 013801.
[30] H. Gu, B. Ye, H. Ding, C. Liu, Y. Zhao, Z. Gu, Non-iridescent structural color pigments from liquid marbles, J. Mater. Chem. C 3 (2015) 6607–6612.
[31] Y. Takeoka, Angle-independent structural coloured amorphous arrays, J. Mater. Chem. 22 (2012) 23299–23309.
[32] S. Yoshioka, Y. Takeoka, Production of colourful pigments consisting of amorphous arrays of silica particles, ChemPhysChem 15 (2014) 2209–2215.
[33] L. Shi, Y. Zhang, B. Dong, T. Zhan, X. Liu, J. Zi, Amorphous photonic crystals with only short-range order, Adv. Mater. 25 (2013) 5314–5320.
[34] B. Dong, X. Liu, T. Zhan, L. Jiang, H. Yin, F. Liu, J. Zi, Structural coloration and photonic pseudogap in natural random close-packing photonic structures, Opt. Express 18 (2010) 14430–14438.
[35] H. Wang, K.-Q. Zhang, Photonic crystal structures with tunable structure color as colorimetric sensors, Sensors 13 (2013) 4192–4213.
[36] C.I. Aguirre, E. Reguera, A. Stein, Tunable colors in opals and inverse opal photonic crystals, Adv. Funct. Mater. 20 (2010) 2565–2578.
[37] S.J. Woltman, G.D. Jay, G.P. Crawford, Liquid-crystal materials find a new order in biomedical applications, Nat. Mater. 6 (2007) 929–938.
[38] A. Yadav, R. De Angelis, M. Casalboni, F. De Matteis, P. Prosposito, F. Nanni, I. Cacciotti, Spectral properties of self-assembled polystyrene nanospheres photonic crystals doped with luminescent dyes, Opt. Mater. 35 (2013) 1538–1543.
[39] M. Haque, G. Kamita, T. Kurokawa, K. Tsujii, J.P. Gong, Unidirectional alignment of lamellar bilayer in hydrogel: one-dimensional swelling, anisotropic modulus, and stress/strain tunable structural color, Adv. Mater. 22 (2010) 5110–5114.
[40] J.D. Forster, H. Noh, S.F. Liew, V. Saranathan, C.F. Schreck, L. Yang, J.G. Park, R.O. Prum, S.G. Mochrie, C.S. O'Hern, Biomimetic isotropic nanostructures for structural coloration, Adv. Mater. 22 (2010) 2939–2944.

[41] Y. Zhang, B. Dong, A. Chen, X. Liu, L. Shi, J. Zi, Using cuttlefish ink as an additive to produce non-iridescent structural colors of high color visibility, Adv. Mater. 27 (2015) 4719–4724.
[42] K. Chung, S. Yu, C.J. Heo, J.W. Shim, S.M. Yang, M.G. Han, H.S. Lee, Y. Jin, S.Y. Lee, N. Park, Flexible, angle-independent, structural color reflectors inspired by morpho butterfly wings, Adv. Mater 24 (2012) 2375–2379.
[43] D. Ge, L. Yang, G. Wu, S. Yang, Spray coating of superhydrophobic and angle-independent coloured films, Chem. Commun. 50 (2014) 2469–2472.
[44] L. Cui, Y. Zhang, J. Wang, Y. Ren, Y. Song, L. Jiang, Ultra-fast fabrication of colloidal photonic crystals by spray coating, Macromol. Rapid Commun. 30 (2009) 598–603.
[45] M. Harun-Ur-Rashid, A. Bin Imran, T. Seki, M. Ishii, H. Nakamura, Y. Takeoka, Angle-independent structural color in colloidal amorphous arrays, ChemPhysChem 11 (2010) 579–583.
[46] A. İncel, T. Güner, O. Parlak, M.M. Demir, Null extinction of ceria@ silica hybrid particles: transparent polystyrene composites, ACS Appl. Mater. Interfaces 7 (2015) 27539–27546.
[47] F. Wang, X. Zhang, Y. Lin, L. Wang, J. Zhu, Structural coloration pigments based on carbon modified ZnS@ SiO2 nanospheres with low-angle dependence high color saturation, and enhanced stability, ACS Appl. Mater. Interfaces 8 (2016) 5009–5016.
[48] I. Lee, D. Kim, J. Kal, H. Baek, D. Kwak, D. Go, E. Kim, C. Kang, J. Chung, Y. Jang, Quasi-amorphous colloidal structures for electrically tunable full-color photonic pixels with angle-independency, Adv. Mater. 22 (2010) 4973–4977.
[49] W. Stöber, A. Fink, E. Bohn, Controlled growth of monodisperse silica spheres in the micron size range, J. Colloid Interface Sci. 26 (1968) 62–69.
[50] C.C. Carcouët, M.W. van de Put, B. Mezari, P.C. Magusin, J. Laven, P.H. Bomans, H. Friedrich, A.C.C. Esteves, N.A. Sommerdijk, R.A. van Benthem, Nucleation and growth of monodisperse silica nanoparticles, Nano Lett. 14 (2014) 1433–1438.
[51] M.M. Demir, R. Muñoz-Espí, I. Lieberwirth, G. Wegner, Precipitation of monodisperse ZnO nanocrystals via acid-catalyzed esterification of zinc acetate, J. Mater. Chem. 16 (2006) 2940–2947.
[52] Y. Takeoka, M. Honda, T. Seki, M. Ishii, H. Nakamura, Structural colored liquid membrane without angle dependence, ACS Appl. Mater. Inter. 1 (2009) 982–986.
[53] N. Kumano, T. Seki, M. Ishii, H. Nakamura, Y. Takeoka, Tunable angle-independent structural color from a phase-separated porous gel, Angew. Chem. Int. Ed. 50 (2011) 4012–4015.
[54] J.G. Park, S.H. Kim, S. Magkiriadou, T.M. Choi, Y.S. Kim, V.N. Manoharan, Full-Spectrum photonic pigments with non-iridescent structural colors through colloidal assembly, Angew. Chem. Int. Ed. 53 (2014) 2899–2903.
[55] H. Noh, S.F. Liew, V. Saranathan, R.O. Prum, S.G. Mochrie, E.R. Dufresne, H. Cao, Double scattering of light from biophotonic nanostructures with short-range order, Opt. Express 18 (2010) 11942–11948.
[56] H. Noh, S.F. Liew, V. Saranathan, R.O. Prum, S.G. Mochrie, E.R. Dufresne, H. Cao, Contribution of double scattering to structural coloration in quasiordered nanostructures of bird feathers, Phys. Rev. E 81 (2010) 051923.
[57] S. Magkiriadou, J.-G. Park, Y.-S. Kim, V.N. Manoharan, Absence of red structural color in photonic glasses, bird feathers, and certain beetles, Phys. Rev. E 90 (2014) 062302.